In situ flow cell platform for examining calcium oxalate and calcium phosphate crystallization on films of basement membrane extract in the presence of urinary 'inhibitors'

Cary A. Kuliasha, Douglas Rodriguez, Archana Lovett, and Laurie B. Gower

Electronic Supplementary Information

AU Solution Stability

The AU solutions used for this work to form CaOx crystals contained a variety of chemicals including both $CaCl_2$ and NaH_2PO_4 and their respective ions, and it was possible that the saturated solutions could form off-target CaP within the beakers before travelling through the flow-cell (section 2.4). For this reason, NaH_2PO_4 was only added to the $CaCl_2$ AU solution immediately before adjusting pH to 6.0, and control experiments were performed to confirm that the pH was stable and no detectable amounts of off-target CaP formed in any of the solutions for the duration of the experiments. Solutions were prepared as described in section 2.2 and stored at 37 ˚C in an incubator for 48 hours. Solutions were periodically removed, pH was measured (*Accumet AB200* meter with an *Orion P156D JWP* probe*, Fisher Scientific)*, and were returned to the incubator (ESI Fig. S1). For the 12 solution types measured, pH fluctuated around 5.99 ± 0.11 over the course of 48 h, and both NaOx and $CaCl_2$ AU solutions remained optically clear with no detectable CaP from centrifuged and purified remains. The 50/50 NaOx + $CaCl_2$ solutions formed expected CaOx crystals with no identifiable CaP. On the other hand, solution pH was adjusted to 7.5, as opposed to 6.0, to intentionally form CaP on the flow-cell BME substrate (section 2.5).

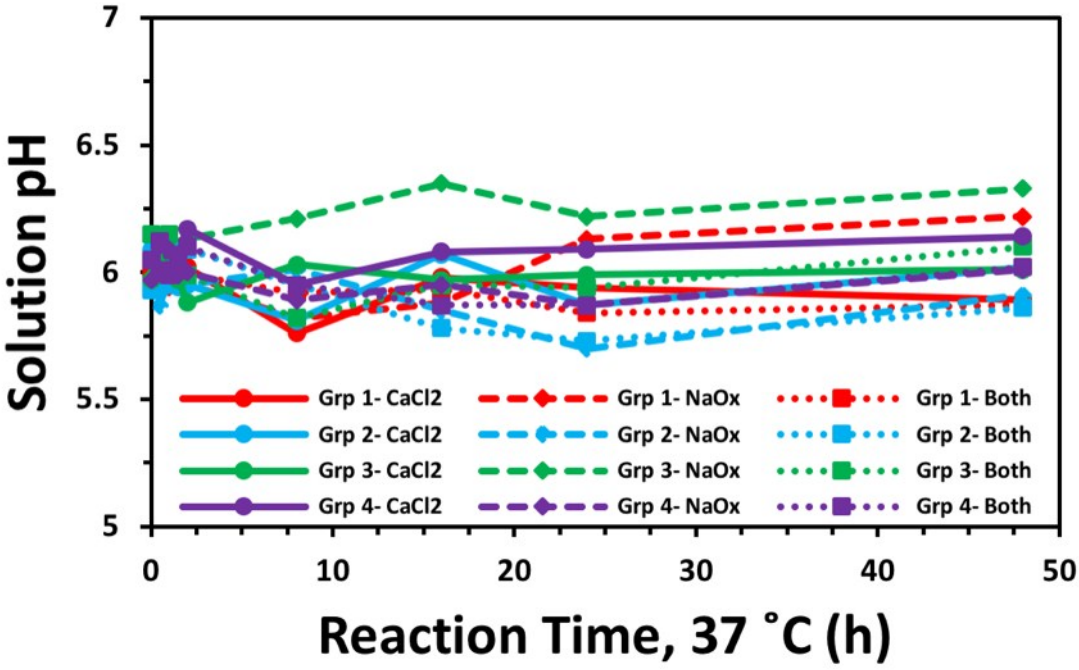

ESI Figure S1. Solution pH at 37 ˚C remained stable around 5.99 ± 0.11 and no significant trending changes were observed. Measurements were taken at time 0, 0.5, 1, 1.5, 2, 8, 16, 24, and 48 h.

Flow-Cell Assembly Details

The flow-cell assembly was fabricated using two standard 75 x 25 mm glass-slides and a molded PDMSe gasket (ESI Fig. S2). A Dremel tool was used to cut ~ 3-4 mm diameter holes into the glass-slide of the flow-cell top. The first ~5 mm from tips of 25-µL pipettes were manually cut using a razor blade, and the remaining pipette bases were inserted into the cut holes to act as mounting points for the Tygon tubing (4 mm ID inlet port and 6 mm outlet port). These attachment points were secured and sealed to the flow-cell top using PDMSe.

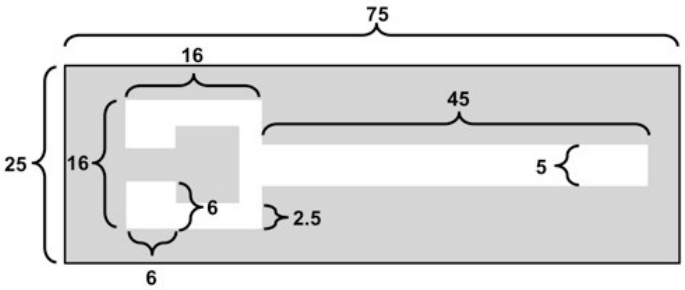

ESI Figure S2. Schematic of the PDMSe gasket (grey) showing relevant dimensions of the flow-cell regions (white). All dimensions are in mm.

Basement Membrane Extract (BME)

The BME is a commercially available hydrogel (purified from Engelbreth-Holm-Swarm tumor), and is composed primarily of laminin, collagen IV, entactin, and heparan sulfate proteoglycan. The dehydrated BME was analyzed via SEM without the presence of any CaOx crystals or other salts to determine its general morphology (ESI Fig. S3). Swollen hydrated thickness was estimated to be 360 ± 270 µm using contact profilometry (*Dektak 150, Veeco*); however, this method requires a physical stylus to make contact with the surface of the BME at 1 mg of force. It is likely that the BME was compressed during measurements and the thickness values should only be considered rough approximations. The theoretical BME thickness formed after applying 75 µL of BME onto the 45 mm x 5 mm flow cell region is approximately 333 µm. This value roughly equates to the contact profilometry measurements.

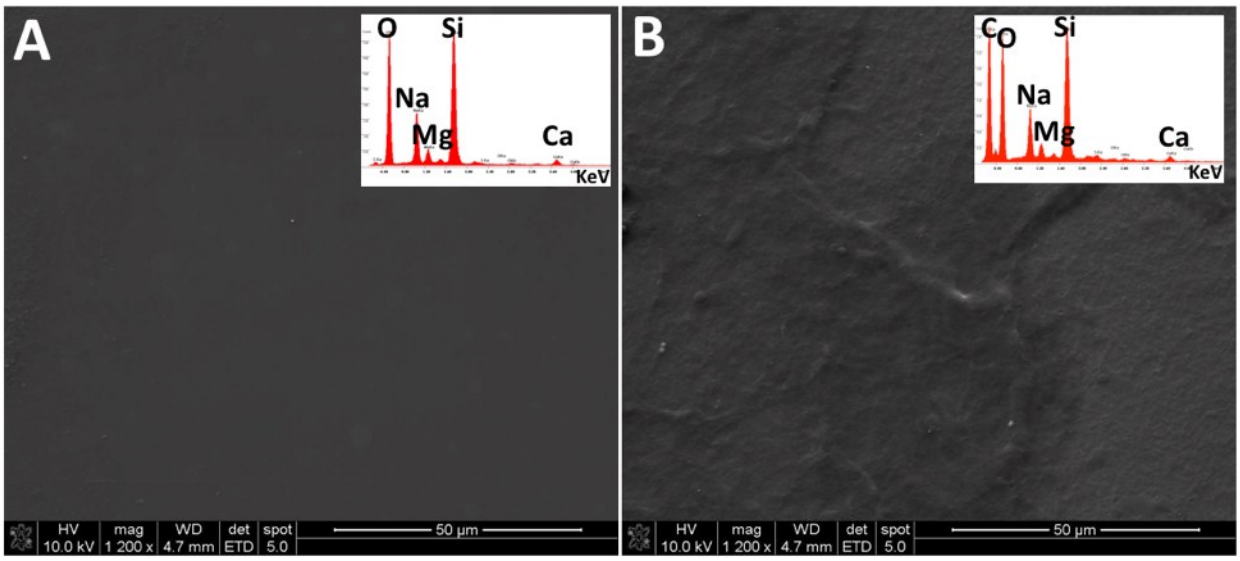

ESI Figure S3. SEM micrographs of a (A) bare glass slides and (B) a glass slide with dehydrated BME. The BME can be easily detected from its morphological profile (typical of a dehydrated hydrogel) and from the presence of carbon in the EDS spectra (insets) from the organic constituents of the BME.

CaOx Crystallization Location Within/ On the BME hydrogel

During flow-cell experiments, the BME is fully hydrated into a swollen hydrogel and the AU solutions can easily permeate its network. Therefore, crystals could form both on the BME surface or within its bulk. It is exceedingly difficult to accurately identify the specific Z-axis location of formed crystals *in situ* using optical methods due to the only slight difference in optical focus. However, we believe that SEM analysis was able to identify crystal formation locations by closely inspecting the surface morphology of crystals (ESI Fig. S4). Crystals that formed on top of the BME surface had clearly identifiable surface features and texturing (e.g., plates, cracks, edges). Crystals that formed within the bulk of the BME were coated with a layer of BME that smoothed and masked specific details on the crystal surface. Furthermore, a BME meniscus layer could be identified between multiple BME coated crystals or around the base of the crystal.

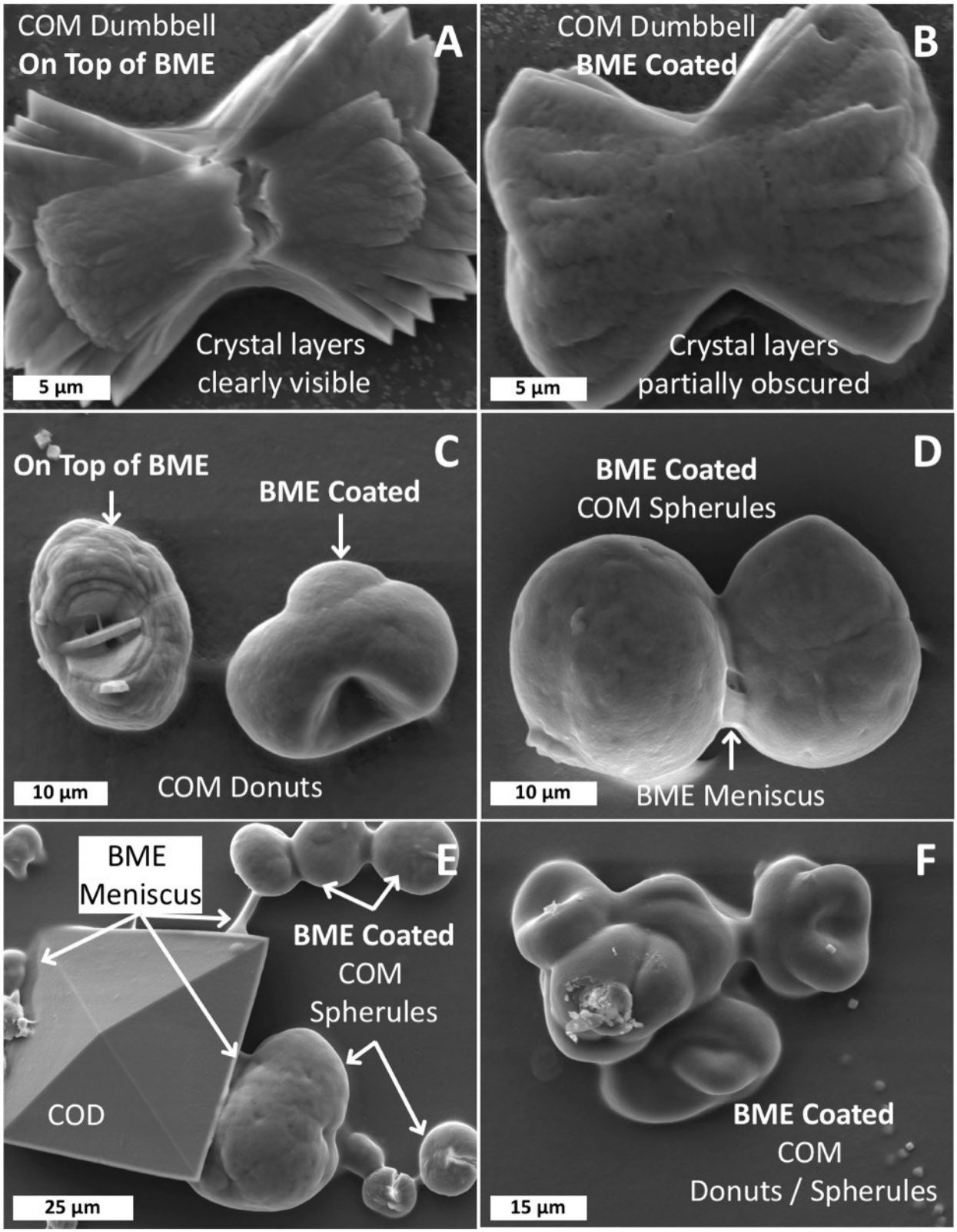

ESI Figure S4. SEM micrographs of CaOx crystals that formed either on the BME surface or within the bulk of the BME gel. (A-B) Group 1 formed COM dumbbells, and (C-F) group 4 formed COM donuts/ spherules and COD bipyramids. The location of the BME is indicated as well as highlights to the BME meniscus that forms around BME coated crystals.

***In Situ* Flow-Cell Time-Lapse Crystallization**

A primary advantage of the flow-cell platform is the ability to capture time-lapse images of the crystal nucleation and growth *in situ*. This allows for individual crystals to be monitored over long durations (hours) with relative ease. Each AU group was investigated using this method. Group 1-2 solutions rapidly formed COM dumbbells and coffins as explained in the text, and some time-lapse snapshots are presented to highlight areas of interest (ESI Fig. S5). COM tablet formation was captured during group 3 experiments (ESI Fig. S6).

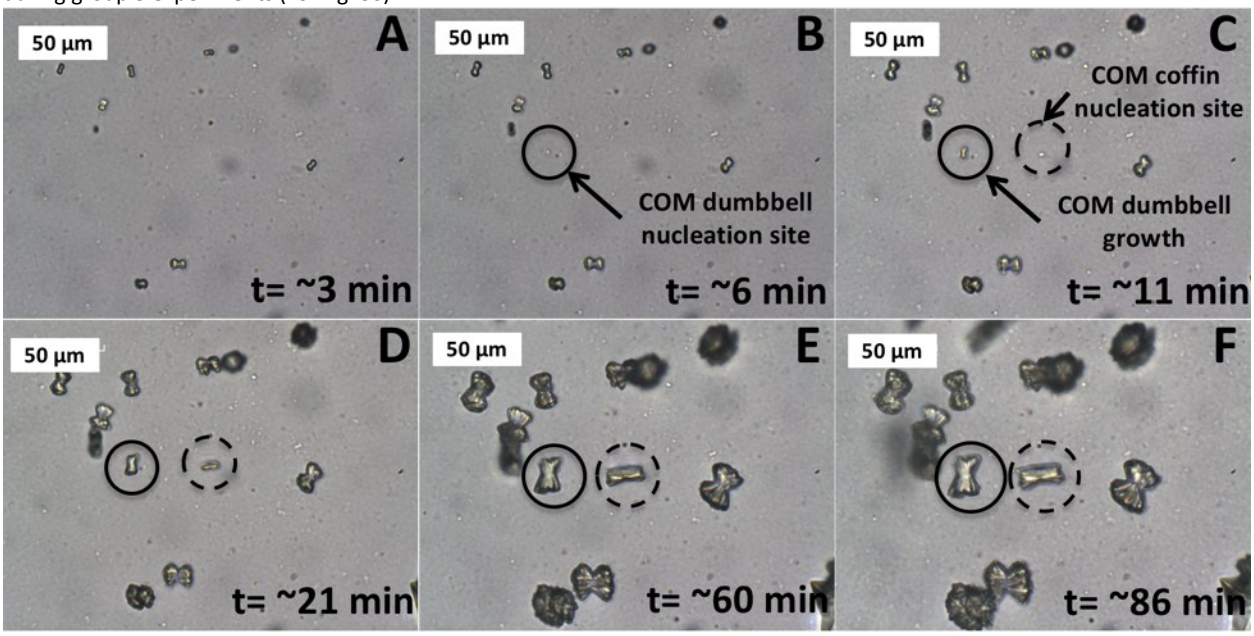

ESI Figure S5. Representative time-lapse images of group 1-2 flow-experiments. (A) Small COM crystals form after ~3 min of AU flow (already demonstrating the dumbbell splitting pattern), and (B-C) additional nucleation events can be captured, and (D-F) the crystal growth can be followed. For this example, no COD crystals were observed during these initial time-points

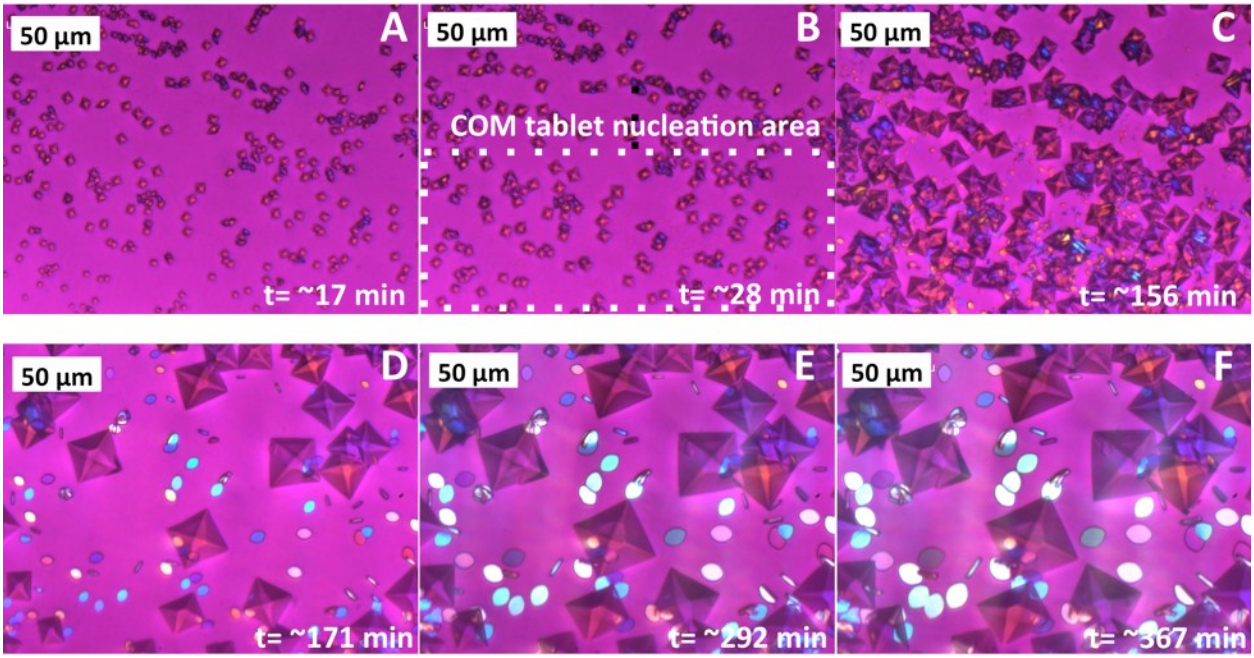

ESI Figure S6. Representative time-lapse images of group 3 flow-experiments. (A) Small COD bipyramid crystals form after ~15 min of AU flow, and (B) COM tablet nucleation events can be captured and (C-F) the crystal growth can be followed.

Group 4 AU Crystallization and COM Donut/ Spherule Formation

COM formed using group 4 AU solutions with Mg^{2+}, citrate, and OPN exhibited a central depression along the (100) face. SEM analysis indicates that radially stacked CaOx crystalline plates form the depression (ESI Fig S7). With these COM "donuts," the central depression (i.e., donut hole) eventually is fully filled with the radially stacked CaOx plates resulting in a COM spherule. Time-lapse imaging at RT was able to identify COM donut formation progressing to spherule growth (ESI Fig. S8).

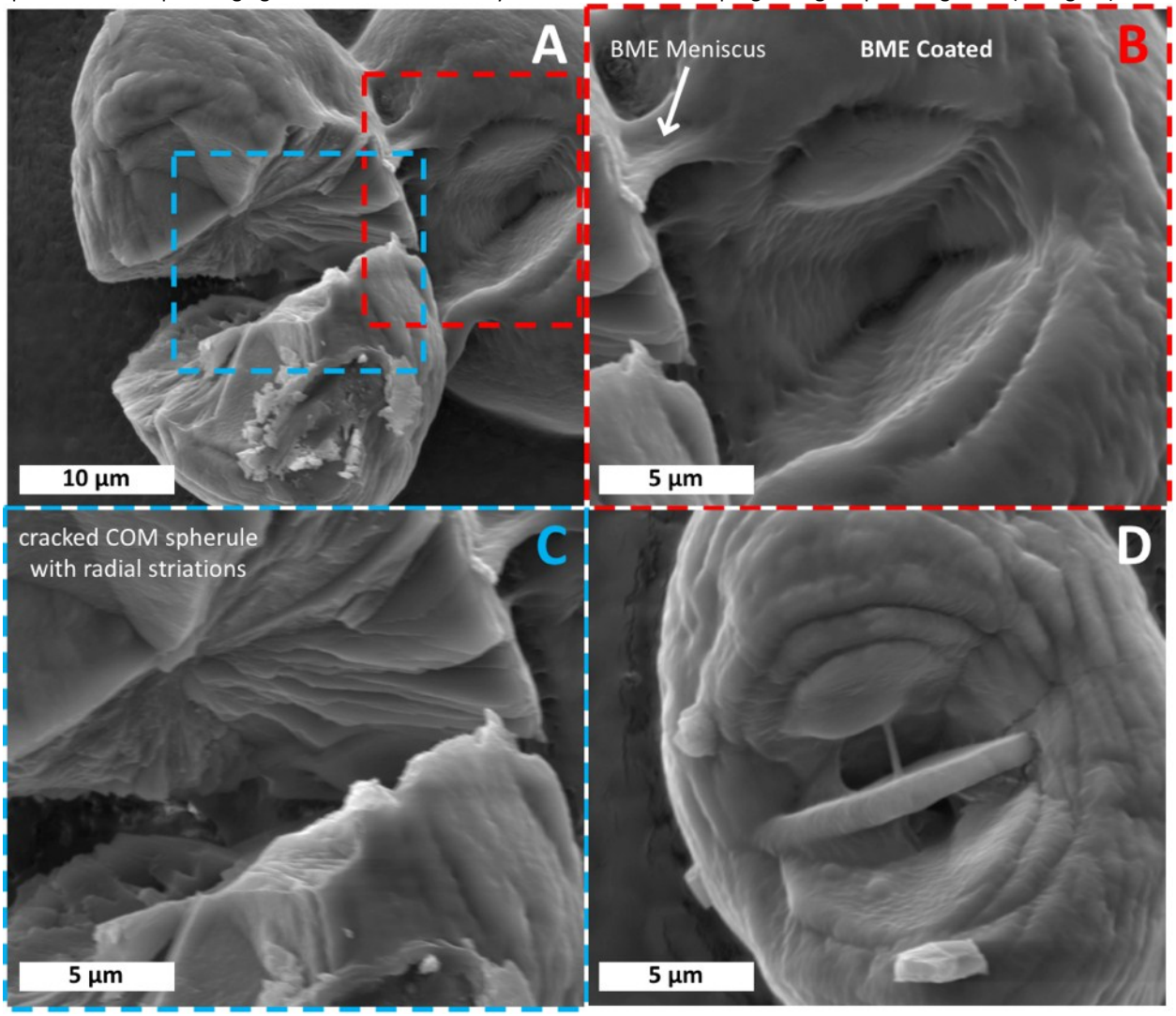

ESI Figure S7. Representative SEM images highlighting the central depression of group 4 formed COM donuts. The central depression along the (100) axis is prevalent. (A) two COM donuts, and (B-C) zoomed in regions of the central depression from (A) highlighting both the radially stacked plates (B) and the inner morphology of a cracked crystals (C). (D) An additional COM donut with what appears to be a partially formed COM crystalline plate within the central (100) depression.

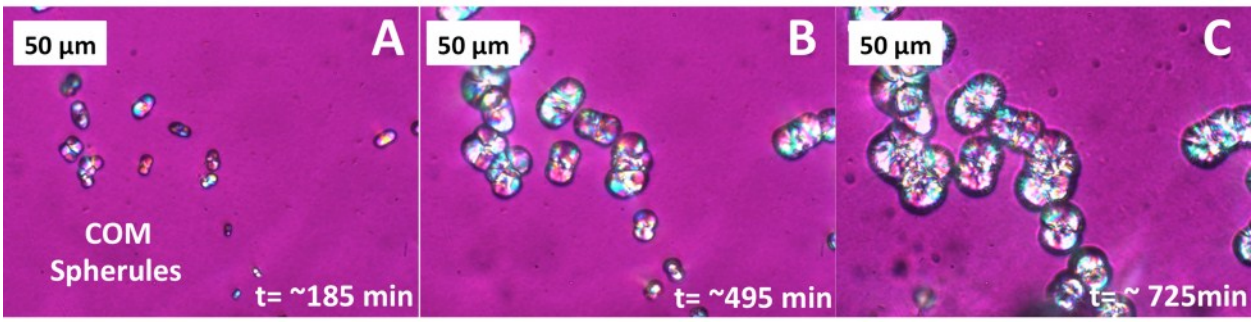

ESI Figure S8. Representative time-lapse images of group 4 flow-experiments showing (A) small COM donuts after initial nucleation with the characteristic dimple along the (100) face that proceed (B-C) to grow into fully formed spherules.

CaP Crystallization

CaP crystallization on the BME substrates was analyzed with optical, SEM, and Raman spectroscopy to confirm the physical and chemical structure of the CaP films (ESI Fig. S9). It is apparent from SEM analysis that the CaP formed both on the surface of the BME (ESI Fig. S9 C) and within the bulk of the BME (ESI Fig. S9 D). The CaP mineral was similar to that seen in the literature for hydroxyapatite nucleated on a variety of substrates, where platelets tend to grow roughly orthogonal to the substrate, and/or are bundled into loosely packed spherulites, although the platelets appear somewhat more wavy and irregular. Experiments that utilized CaOx AU solutions in conjunction with previously crystallized CaP/ BME substrates resulted in CaOx crystals consistent with those found without the presence of CaP (ESI Fig. S10). Raman spectra of these structures have also been included (ESI Fig. S11)

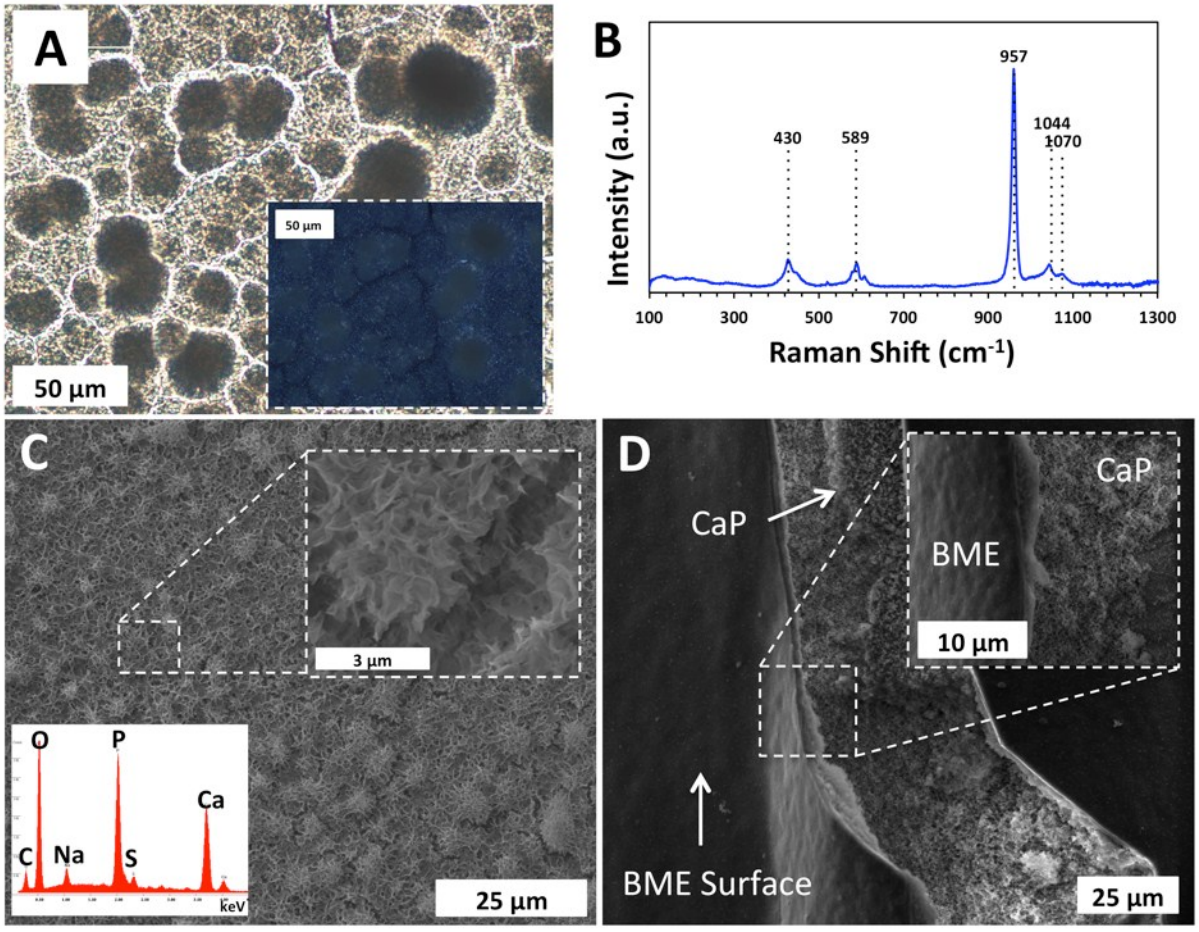

ESI Figure S9. Characterization of CaP films formed on BME. (A) Optical image showing general structure of the heavily mineralized CaP film. The CaP layer fractured during dehydration. Cross-polarized images (inset) confirms CaP crystallinity, although the birefringence appears weak due to the thickness of the film and small size of the crystallites. (B) Raman spectra identifying the CaP film as hydroxyapatite. (C-D) SEM micrographs showing both (C) CaP formation on the surface of the BME substrate and (D) within the bulk of the BME. Insets shows higher magnification regions of interest and EDS spectra of CaP.

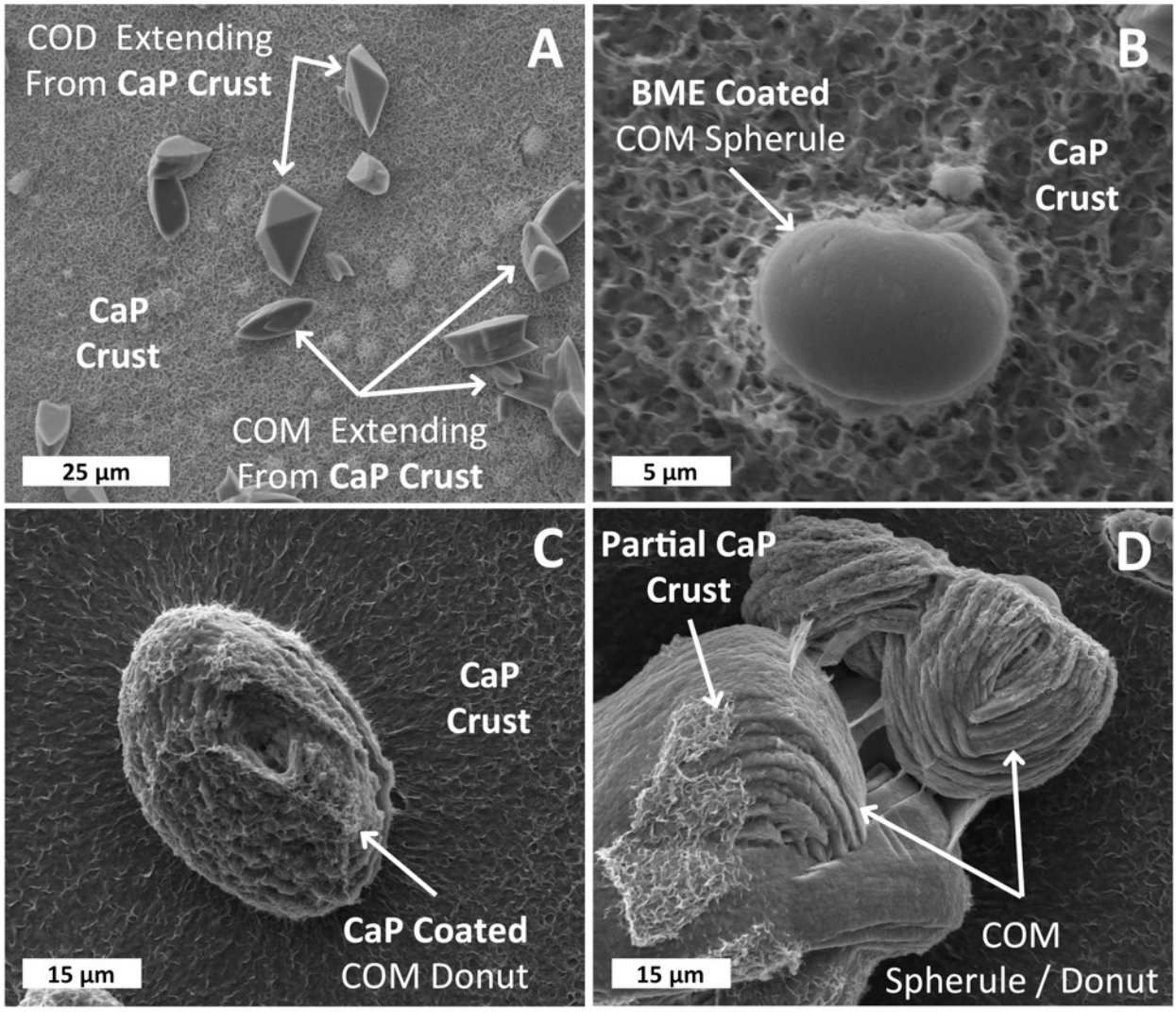

ESI Figure S10. CaP + CaOx flow-cell crystallization results highlighting the relative formation of CaOx with respect to the underlying CaP layer. (A) Group 1 CaOx formation of COD bipyramids and COM coffins that are partially extended from the CaP surface. CaOx crystals are partially obscured by CaP suggesting that the remainders are buried underneath. (B) Group 4 COM spherule that formed on top of the surrounding CaP surface, and (C) Group 4 COM donut that formed underneath the CaP surface as evidenced by its plate-like CaP coating. (D) Cluster of group 4 COM spherules with residual CaP crust likely remaining after the CaOx crystals broke free of the CaP underlay.

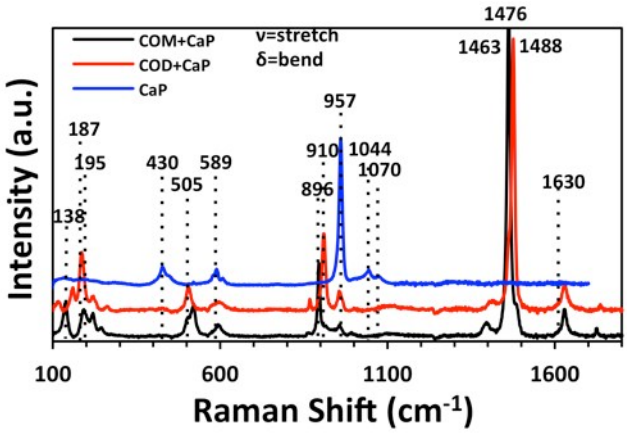

ESI Figure S11. CaP + CaOx Raman analysis showing expected constituent peaks.